Characterization of Stronghold Fortifications by 2D/3D/4D Electrical Resistivity Tomography: Major Push Towards Quantitative Interpretation

RADEK KLANICA,[1] Ivo ŠTEFAN,[2] JAN HASIL,[3] and ROMAN BERÁNEK[1]

Abstract—Geophysical methods are widely used as noninvasive tools for archaeological prospection. In a first step is usually applied basic prospection of vast areas, when data are evaluated only in qualitative way. Sometimes is performed second step, during which take place more detailed multidimensional or combined surveys in order to image archeological monuments complexly, allowing quantitative interpretation. Hence, we used a unique and novel combination of multidimensional electrical resistivity tomography (ERT) on the Early Middle Ages stronghold fortifications at Vinoř (Czechia) to achieve such interpretation. The joint results of 2D/3D/4D (time-lapse) surveys allowed us to precisely characterize individual construction components of the fortifications, including a ditch and rampart enhanced by a front wall with a berm. The ERT results recovered the fortification dimensions and the volume of building material used. The surveyed fortification section was verified by excavations directly after the ERT measurements. A comparison of the excavated section with geophysics proved that ERT was able to infer all the important fortification characteristics. In addition, illustrative picture of the resistivity manifestations of the basic components of this very typical fortification construction were obtained. The results show that multidimensional ERT provide access to quantitative interpretation allowing to explain archaeological structures behind investigated anomalies. In result, sites containing cultural heritage can be leaved intact, excavations can be substituted in surprisingly large extent, while unprecedented amount of archaeological information is still retrieved.

Keywords: Stronghold, fortification, Electrical Resistivity Tomography, quantitative, 4D ERT, archaeology.

[1] Institute of Geophysics of the CAS, Boční II/1401, Prague 4, Czech Republic. E-mail: rk@ig.cas.cz; beranek@ig.cas.cz
[2] Faculty of Arts, Charles University, Celetná 20, Prague 1, Czech Republic. E-mail: ivo.stefan@ff.cuni.cz
[3] Institute of Archaeology of the CAS, Prague, Letenská 4, Prague 1, Czech Republic. E-mail: hasil@arup.cas.cz

1. Introduction

Geophysical methods have been proved essential tools for nondestructive research in archeology in recent years (e.g., Cau-Ontiveros et al., 2023; Cowan et al., 2022; De Smedt et al., 2022; Jeon et al., 2022; Krivanek, 2021; Kuna et al., 2021; Pasteka et al., 2020; Stele et al., 2022; Wallner et al., 2022). They have the capacity to reveal archeological features in a detailed manner, while preserving the site intact. However, geophysical methods can be used in two ways in archaeological prospection. When they are applied for the basic prospection of vast areas, only minority of anomalies can be excavated and verified. In such case only quantitative interpretation is often obtained and anomalies are interpreted as shapes or contours. More information about the anomalies as depth, exact dimensions in 3D or physical properties of anomalies is hard to assess (nevertheless even qualitative interpretation is valuable in archaeological sense). Qualitative interpretation is often desirable in case of spatially large settlements, where can geophysical methods map entire archaeological sites and effectively target more detailed surveys or subsequent excavations. Such approach is used to reveal extent and inner structure of cities, castles, hillforts or inhabited places in general. This is done mostly by geophysical methods allowing quick data acquisition on large area as magnetometer surveys, frequency-electromagnetics (FDEM), or georadar (GPR).

Quantitative interpretation goes further, relates anomalies with physical properties (e.g. resistivity) and describes actual structures behind the data (Zhang et al., 2011). For obtaining such information, individual geophysical methods need to be combined or complexly designed surveys of single methods

have to be used. These usually include combinations of 2D and 3D layouts using magnetometer/FDEM surveys, GPR, Electrical Resistivity Tomography (ERT) and drillings. Different studies used such strategy, for example: GPR with drillings to reconstruct Mesolithic hunter-gatherer site (Corradini et al., 2020); 3D GPR with airborne laser scanning to investigate protohistoric burial mound and hillfort (Bernardini et al., 2021); FDEM and magnetometry to image Roman villa (Rizzo et al., 2023); FDEM, GPR, ERT and magnetometry to image and understand Roman city (Mozzi et al., 2016); FDEM and ERT to reconstruct paleo landscape in vicinity of Roman harbor (Casas et al., 2021) or ERT, GPR and seismic refraction for reconstruction of Bronze Age mine (Trebsche et al., 2022). Broad complex of geophysical methods is also often coupled with other scientific methods as geomorphology, sedimentology, paleontology or oceanography to support geophysical outcomes as e.g. in case of Desruelles et al. (2023), who reconstructed harbor of the Ancient Greek city.

ERT is a direct-current method used for inferring subsurface electrical resistivity. In principle, an electrical current I (A) is injected into the ground through two steel electrodes (C1–C2), while the potential difference U (V) is measured between another pair of electrodes (P1–P2). By considering the geometry factor of the electrode array k, the apparent resistivity can be obtained through a modified Ohm's law, $\rho_z = kU/I$. Subsequently, ρ_z has to be transformed to the real resistivity ρ of the environment by a so-called inversion process, by which an inversion program tries to find a resistivity model explaining the measured data (e.g., Ellis & Oldenburg, 1994; Loke, 2020; Loke & Barker, 1996; Parker, 1994). This process is performed through iterative, nonlinear, regularized inversion algorithms conducted in different programs (e.g., Res2Dinv, BERT) in 2D (profile), 3D (cube), or 4D (time-lapse).

ERT has been successfully used for a variety of archaeological targets, including walls, pits, ditches, burial mounds, foundations or water tanks (e.g., AL-Hameedawi et al., 2022; Al-Saadi et al., 2018; Grison et al., 2022; Nowaczinski et al., 2012, 2015; Zhao et al., 2019). Despite the fact that ERT is not commonly used and is not very suitable for spatial surveys, it is well-designed for the imaging of well-defined individual targets, such as fortifications. ERT has been applied for the prospecting of both ramparts and ditches (e.g., Hegyi et al., 2018; Nowaczinski et al., 2012), but commonly applied 2D surveys investigate fortifications as a complement to spatial magnetometer and GPR surveys. Some 2D studies have explored the capabilities of ERT in stronghold and hillfort fortification imaging in detail (Klanica et al., 2022b) or have tried to exactly compare observed resistivity anomalies with archeological excavations (Milo et al., 2020 and 2022). Surveying fortifications in 3D is still rarely undertaken (Di Maio et al., 2016; Klanica et al., 2022a), although it offers a unique view of the subsurface and allows constraining resistivity images in space. Time-lapse surveys (called 4D) are very rare in archaeology (Ranieri et al., 2007), since there is usually limited time for geophysics before excavations. Although, 4D allow the evaluation of resistivity anomalies under different moisture conditions and, thus, observation of the changing extent of individual anomalies over time. 4D surveys are commonly applied to landslides (Holmes et al., 2020), hydrogeology (McLachlan et al., 2020; Uhlemann et al., 2022) or permafrost studies (Uhlemann et al., 2021).

From the chalcolithic period to the Early Middle Ages, fortified central places known as strongholds or hillforts were built throughout Europe (Salač et al., 2019). Although constructed at strategic places protected by natural elements, the defense of such sites was usually enhanced by man-made defensive lines. Fortifications can have numerous shapes and sizes, given the age of origin, culture, location, and importance of a particular site (Christensen, 2004; Oliva, 2004; Parkinson & Duffy, 2007; Zotti & Neubauer, 2011). Analyses of fortification construction offer deeper insight into the engineering skills of builders and their socio-economic relations, while inferred labor investments illustrate the complexity of past societies (e.g., Abrams & McCurdy, 2019; Jo et al., 2018). However, important evidence has to be gathered, including the building materials used and their volumes, the sizes and shapes of ramparts and ditches, and the complexity of individual building components (e.g., Nowaczinski et al., 2013; Pickett et al., 2016).

The main aim of this study was to push ERT beyond the basic description of resistivity anomalies towards quantitative interpretation by use of multi-dimensional surveys. Consequently, verification of the ERT results through excavations allow to establish better connections between resistivity images and archaeological features. The results are presented and discussed for stronghold Vinoř (Czechia), belonging to the one of the power centers of the Přemyslid dynasty at the turn of the first millennium. The fortification line delimiting the bailey, which consists of a rampart and a ditch, was prospected using a combination of 2D, 3D, and 4D ERT surveys with different settings under different moisture conditions. Later, for verification of the ERT results, the examined fortification section was manually dismantled, excavated, and analyzed by means of archaeology. The presented approach shows that quantitative interpretation can be accessed via multidimensional ERT, while amount of archaeological information gained can be significantly increased compared to 2D profiling. Study also introduces an unusual approach using various multidimensional ERT surveys including the novel use of a 4D time-lapse survey for the improvement of interpretation.

2. Study Site

Stronghold Vinoř is located at the northeastern border of Prague (Fig. 1A) within the Cretaceous sandstones covered by Quaternary loess. The stronghold lies on a distinct promontory elongated in the north–south direction above the conjunction of two small valleys that border the promontory from the east, north, and west with $\sim$ 20 m of elevation difference. Only to the south is the area of the stronghold open to flat terrain without any natural borders (Fig. 1b).

The stronghold can be divided into an acropolis and a bailey (Fig. 1B). The acropolis covers the promontory with a total area of 3.7 ha, which is beside natural, steep slopes bordered also by the remains of a rampart with varying heights between 1.5 and 2.8 m. The remains of fortifications on the southern side consist of a $\sim$ 3 m high rampart supplemented by a $\sim$ 2 m deep ditch, and it is assumed that the original entrance to the acropolis was situated here. The total length of the fortification surrounding the acropolis is ca. 760 m. The bailey is located at the southeastern side of the acropolis and encompasses an area of 0.7 ha. It was built in an unusual way, protecting only part of the acropolis without an access road to the main entrance. The bailey is surrounded by fortification remains, which include a $\sim$ 3 m high rampart with a ditch to the west and south, while the eastern side is protected by a $\sim$ 1 m high rampart at the top of an escarpment. The rampart length delimiting the bailey is ca. 280 m, of which 200 m belong to the west and south massive fortification lines.

The promontory was inhabited from the Iron Age (Hallstatt and La Tène cultures), through the Early Middle Ages and Late Middle Ages, up to the Modern Period, according to found archaeological artifacts. The stronghold with the fortification system was probably established at the turn of the ninth and tenth centuries as one of the power centers of the Přemyslid dynasty. This is concluded from the results of several archeological campaigns within the acropolis (Štefan & Hasil, 2023). The rampart bordering the promontory was excavated at its northern end. It was built from earth with a wooden frame and strengthened by a frontal wall. In the northern part of the acropolis were found the remains of a longhouse with dimensions of 9.5 × 40 m, suggesting that the stronghold acted as a regional center of political or social life and not just as a strategic, fortified site.

3. Methods

3.1. ERT Field Setup

ERT data were collected using a five-channel ARES II resistivity system (GF Instruments, Brno, Czech Republic) with a high-density (HD) version of an inverse Wenner–Schlumberger (IWS) electrode array (Loke, 2020). The IWS array was chosen based on tests of different electrode arrays and results from similarly constructed strongholds and hillforts (Klanica et al., 2022a and 2022b). In addition, the IWS array allowed multichannel acquisition and significantly decreased the time required for measurements.
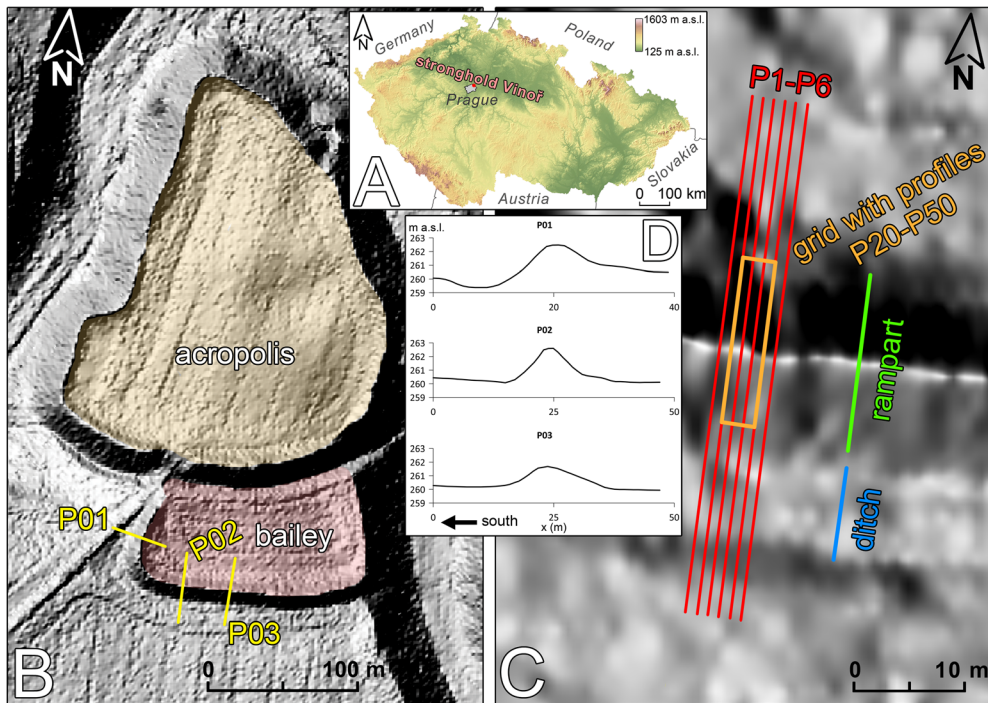
Figure 1
A Schematic map of Czechia showing position of stronghold Prague-Vinoř. **B** Topographic map of the stronghold Vinoř based on LiDAR digital elevation model (CUZK, 2017) with ERT profiles. **C** Closer view of excavated area around P02 with detailed ERT profiles. **D** Elevation profiles of P01-P03 illustrating preserved morphology of the rampart

Some profiles were also measured with a dipole–dipole (DD) array for comparison and validation of the IWS results. The precise position of each profile was obtained using a Trimble R10 GPS receiver, while the topography of the measured profiles and grids was extracted from LiDAR digital elevation model with a mean error height of 0.18 m (CUZK, 2017).

First, three ERT profiles (P01–P03) were measured across the outer rampart of Vinoř stronghold in three different places in order to find the best location to carry out an in-depth investigation (Fig. 1B). The profile lengths were as follows: P01–39 m, P02–47 m, and P03–47 m. The same electrode spacing of 1 m was used. The location of P02 was chosen for detailed surveys after the data analysis (Fig. 1C). A ca. 6 m wide transect across the rampart was pruned and cleaned of bushes, trees, and stumps to allow the accurate placement of 3D ERT grids. So-called quasi-3D surveys (Klanica et al., 2022a; Rödder & Kneisel, 2012) were conducted, which consisted of multiple parallel lines acquired from 2D profiles and subsequently merged into a joint dataset for 3D inversion. The first 3D grid consisted of 6 parallel 47 m long profiles (P1–P6) (P2 = P02) with line and electrode spacings of 1 m. The second, more detailed 3D grid was measured in the central area of a 1 × 1 m grid in order to allow more precise interpretation. It consisted of 7 parallel 15.5 m long profiles (P20–P50) with line and electrode spacings of 0.5 m (P20 = P2; P50 = P5). The x position of 0 m of the detailed profiles (P20–P50) agreed with the x position of 17 m on the longer profiles (P1–P6). Concurrently during the 2D and 3D surveys, data for the 4D time-lapse survey were acquired. The P2 profile was remeasured four times during the year 2022 (2.5., 30.6., 13.7., and 26.7), allowing the capture of resistivity changes induced by rainfall events. The precise precipitation amounts were obtained from an official meteorological station of the Czech Hydrometeorological Institute, which was

located ca. 3 km away from the stronghold. For a summary of the field works, see Table 1.

3.2. ERT Data Processing and Modelling

Acquired data were preprocessed and analyzed for errors. From the ARES II instrument, were downloaded only data points with standard deviations less than 10%. This first step reduced the total number of measured points only regarding units of points. The second step included running preliminary 2D inversions in Res2Dinv (Loke & Barker, 1996; for details of the inversion routine, see, e.g., Loke, 2020), which made it possible to assess RMS error statistics. Points with higher errors than an intuitively selected threshold (usually above 5%) were deleted during this process, while edited data were saved in raw format for final inversions. This approach reduced the number of measured points by about 2%. Generally, the acquired data showed very high quality.

ERT data were processed with different algorithms based on the survey type. Topography based on a LiDAR digital elevation model (CUZK, 2017) was incorporated into all inversion procedures: as X, Z coordinates for 2D and 4D or as an X, Y, Z grid for 3D. All 2D profiles were inverted using the Res2Dinv algorithm and the L2 norm (standard inversion; for use of different norms, see, e.g., Loke et al., 2003) favoring smooth transitions according to our previous works (Klanica et al., 2022b) and expected resistivity contrasts due to local geology. Res2Dinv was chosen for 2D inversions due to its ability to easily assess RMS error statistics. The 3D grids were inverted using the Boundless Electrical Resistivity Tomography package (Günther et al., 2006; Rücker et al., 2006) using tetrahedral cells, which are well-designed for constructing complex, undulating topography in 3D. The 4D time-lapse inversion was carried out in Res2Dinv, because it offers use of time-lapse inversion equation (Kim et al., 2009; Loke et al., 2014), which minimized differences between models at different times. Final inverse models of 2D and 4D surveys were visualized in Surfer (Golden Software, Golden, CO, USA), while 3D grids were analyzed in ParaView (Ayachit, 2015).

3.3. Archaeological Excavations

After the ERT measurements, the fortification section was manually dismantled and documented by drawing, photography, and photogrammetry during a three-week campaign. Found artifacts and ecofacts were collected and are soon to be processed in a laboratory. The excavated area covered a 5 m wide section of rampart, which was uncovered up to the basement loess layer. The ditch was excavated in a 3 m wide section up to a depth of 2.5 m. However, due to its dimensions, its base was not uncovered.

4. Results with Interpretation

4.1. ERT

The inverted ERT profile of P01 (Fig. 2) showed the rampart with a resistivity below 60 Ωm (C1). In front of the rampart was located a presumed ditch (C2) with a lower resistivity around 30–40 Ωm. Behind the rampart was a low-resistivity layer (40–70 Ωm; C3), probably composed of loess. Deeper parts of the profile were represented by higher resistivities (> 300; R1), which coincided with a sandstone

Table 1

Summary of ERT field measurements

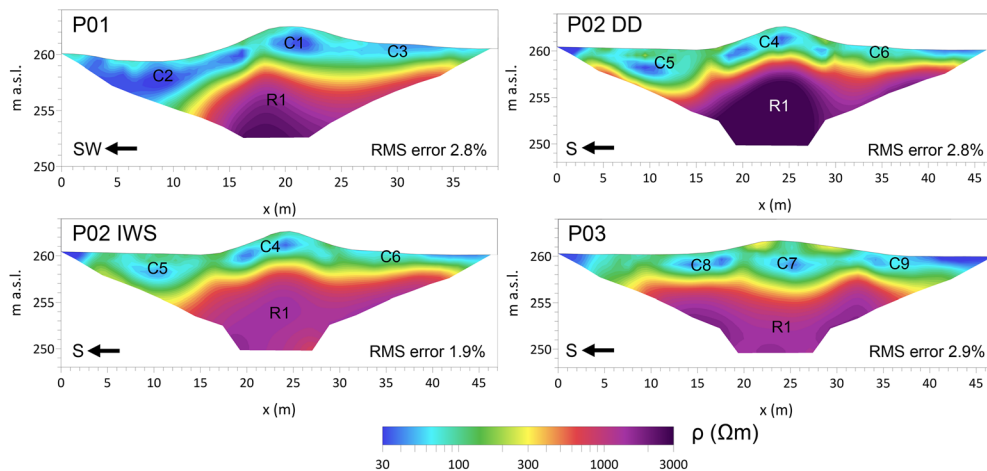| Profile(s)	No. of profiles	Survey	Array	Length	El. spacing
P01…P03	3	2D	IWS/DD	39/47/47 m	1 m
P1…P6	6	2D/3D	IWS	47 m	1 m
P20, P25…P50	7	2D/3D	IWS	15.5 m	0.5 m
4 × P2 (T1-T4)	1 repeated	4D	IWS	47 m	1 m

Figure 2

Inversion results for the first three exploratory ERT profiles. P02 is shown for two electrode arrays: IWS and DD. In general, structures C1, C4, and C7 represent rampart material; structures C2, C5, and C8 identify the ditch; and C3, C6, and C9 indicate the loess layer, with R1 representing the sandstone basement

basement (the same as all other profiles, thus it is not further discussed). The P02 profile identified the same structures with both IWS and DD arrays, but more clearly: the C4 low-resistivity anomaly (30–80 Ωm) represented the rampart material and implied some internal structure; the C5 U-shaped low-resistivity structure (60–80 Ωm) located the ditch with higher precision than on P01; and the C6 low-resistivity layer (40–70 Ωm) coincided with loess cover. It can be seen that differences between the IWS and DD electrode arrays were very low. The distinction between provenance of C4/C5/C6 anomalies was supported mainly by elevation models from LiDAR due to very similar resistivities of the anomalies. The P03 profile showed the same structures, but suggested that the fortifications underwent some additional destruction at this location. After evaluating the results, the P02 area was selected for further surveys.

Figure 3A shows the 2D inversion results for P1 and P6 with a 1 m electrode spacing (for P2–P5, see Supplementary Material) measured around P02. Profiles P1–P6 showed very similar features, so only P1 is described. The rampart could be characterized by low resistivity (30–60 Ωm; C1) and showed two distinct anomalies separated by an area of higher resistivity. While low-resistivity anomalies represented collapsed base material of the rampart, the

area of slightly higher resistivity between them may be attributed to front wall stones. Considering the shape and size of anomalies: in front of the rampart was located a well-defined ditch manifesting low resistivity (< 60 Ωm; C2), while behind the rampart was a low-resistivity loess layer (< 50 Ωm; C3) near the surface. The flat portion of bedrock between ca. 17 and 21 m could be related to the presence of a berm separating the ditch and rampart. An interesting feature is the mid-resistivity anomaly in profiles P1–P3 at the x position of 30 m behind the rampart. It slowly disappeared from P1 to P3 (from west to east) and was most likely related to water drained by the roots of mature trees located in the vicinity of P1.

The results from the 2D inversions of the detailed profiles of P20 and P35 with 0.5 m electrode spacing (Fig. 3B; see Supplementary Material for other profiles) showed closely the internal structure of the rampart. Three distinct low-resistivity anomalies (< 40 Ωm; C1) represented collapsed base material of the rampart. Two anomalies in the outer part of the rampart were separated by an area of higher resistivity (C4), which could be attributed to the presence of front wall stones. Near the surface could be observed multiple anomalies of higher resistivity, which probably corresponded to a weathered topsoil layer. A high-resistivity anomaly (> 200 Ωm; R) could be related to the effect of tree roots, as in the case of P1.
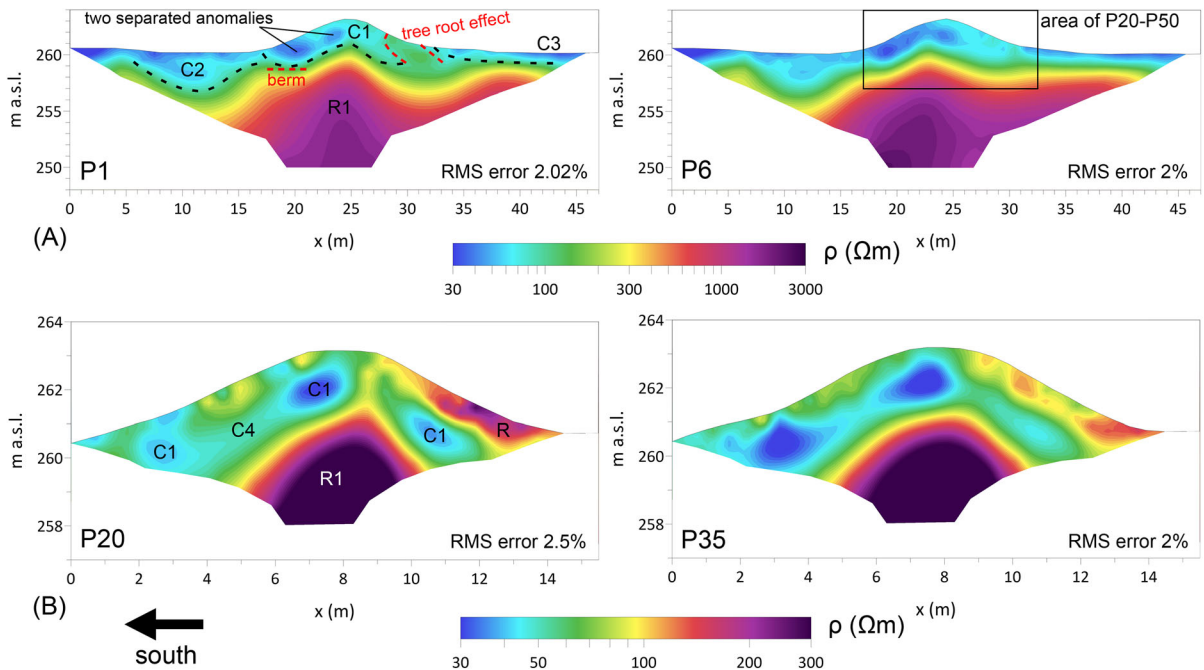
Figure 3

A Inversion results for ERT profiles with 1 m electrode spacing (P1 and P6) from 1 × 1 m grid. All grid profiles identified rampart material (C1) as two separated anomalies, the ditch (C2), a loess layer (C3), and a sandstone basement (R1). **B** Inversion results for ERT profiles with 0.5 m electrode spacing (P20 and P35) from 0.5 × 0.5 m grid. All grid profiles show rampart structure in better detail: rampart material (C1) separated by remains of stone front wall (C4), weathered layer near surface (R), and sandstone basement (R1)

Figure 4A shows the 3D inversion results of merged data from P1–P6, with the lowest achieved RMS error of 2.77%. A cut-through 3D-modeling cube displays the resistivity distribution in 3D, which defined both the ditch and the rampart as low-resistivity zones. Filling of the ditch (Fig. 4B) and building material of the rampart (Fig. 4C) could be isolated from the model based on particular resistivity thresholds (Klanica et al, 2022a). The total volumes for a 1 m wide strip of fortification were estimated to be the following: ca. 25.6 m^3 for excavated material from the ditch and ca. 19.6 m^3 for rampart building material (for more details, see Sect. 5.2).

The inversion results for the 4D time-lapse survey on P2 (Fig. 5) showed significant changes in resistivity during the time induced by precipitation. Major variations in resistivity could be seen in the near-surface layer to a depth of about 1 m. However, noticeable differences in the resistivity of archeological features could be also observed. Measurements at time T1 were conducted after a dryer period,

depicting a clear low-resistivity ditch (< 70 Ωm; C1) and low-resistivity base material of the rampart (< 70 Ωm; C2). Time T2 was measured directly after intense rainfall: 47.7 mm in the previous two days and 94.9 mm in the previous six days. The high amount of precipitation erased the resistivity contrast along the profile and lowered the resistivity of archeological features. The extent of the ditch was hardly recognizable (C1), while the rampart anomaly (C2) significantly increased. The boundary between both features was uncertain. However, anomalies within the rampart were more distinguishable than under dry conditions. Measurements at times T3 and T4 showed slow drying of the profile, which caused higher resistivity contrast, improving conditions for interpretation again.

4.2. Archaeological Excavations

The archaeological excavations of a fortification section yielded the discovery of an extraordinarily
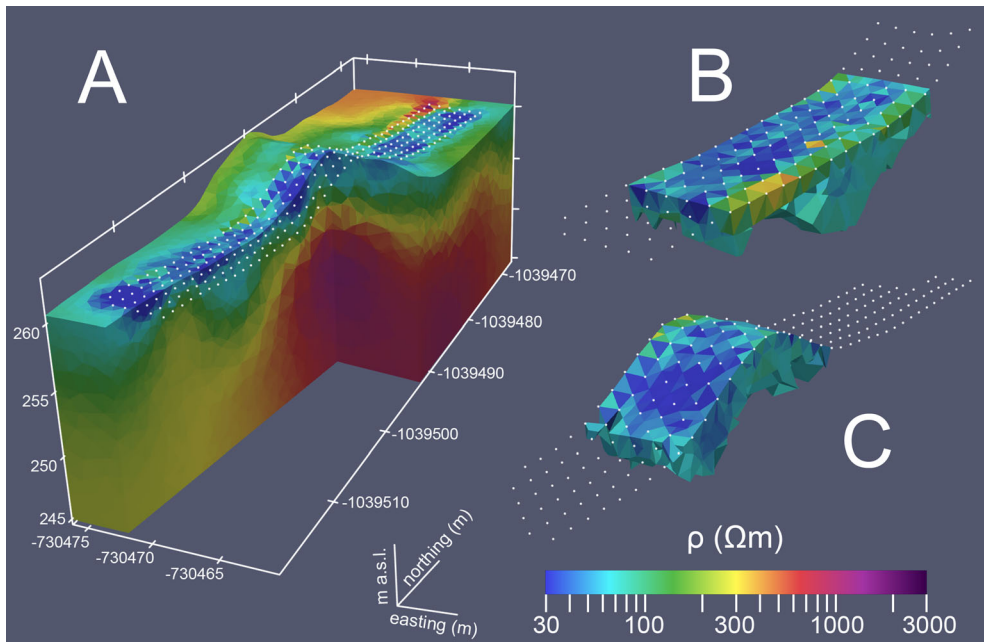
Figure 4

3D inversion results for 1 × 1 m grid built from P1–P6. White dots represent individual positions of electrodes. **A** Entire 3D model showing the resistivity distribution in decadic logarithms within S-JTSK/Krovak, Bpv coordinate frame. **B** Isolated resistivity structure of ditch when a threshold of 80 Ωm was applied. **C** Isolated resistivity structure of rampart when a threshold of 70 Ωm was applied
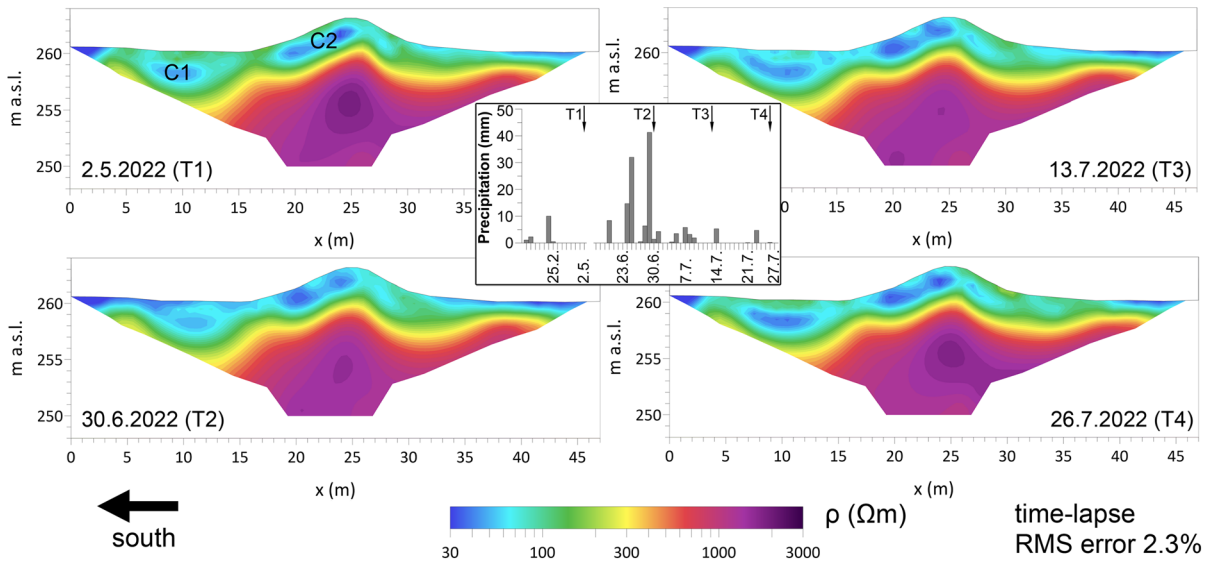

Figure 5

Time-lapse inversion results for ERT P2 profile (P02). Measurements at time T1 were conducted after a dry period and showed maximum resistivity contrast between the ditch (C1) and rampart (C2). Resistivity contrast at time T2 after heavy rainfall was visibly the worst
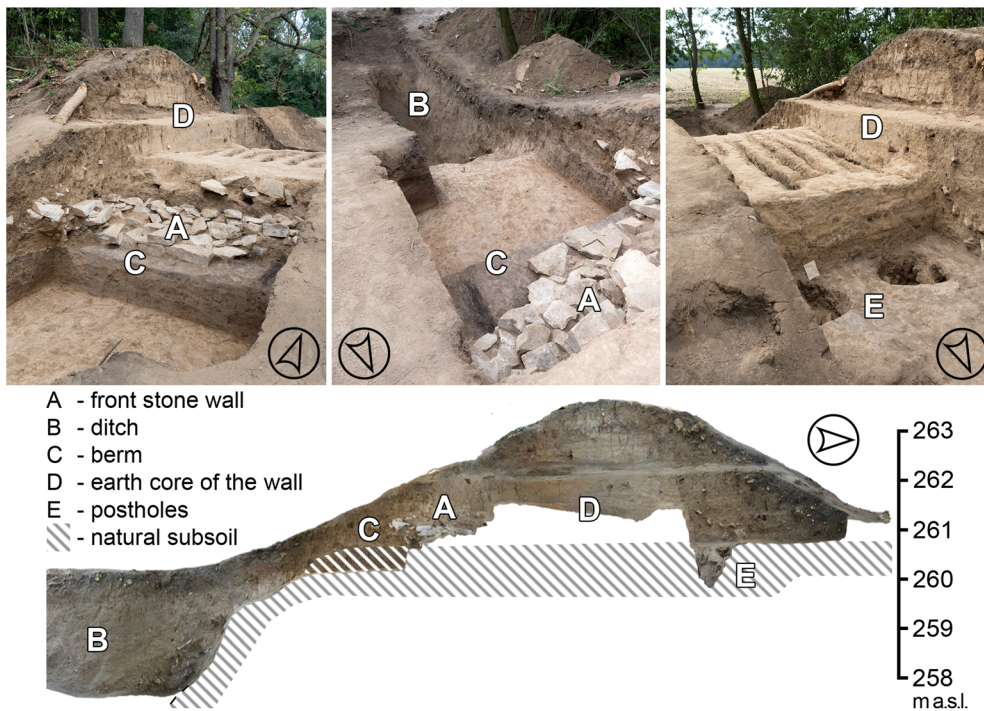
Figure 6

Photographic and photogrammetric documentation of excavation of the outer fortification. Exploratory ERT profiles allowed for optimal section placement of the excavated area to reveal a conclusive and interpretable archeological situation. Photo: R. Klanica; photogrammetry: J. Hasil and D. Pilař

well-preserved early medieval wall (Fig. 6) from the period of the beginning of the Bohemian duchy, i.e., from a time perhaps as early as around 900. A main outcome of the excavations may be considered as the wall in this section never being repaired or damaged by younger anthropogenic activity. This was especially important for interpreting the ERT results. It gave an illustrative picture of the resistivity manifestations of the basic construction components of this very typical construction (ditch, front stone wall, wood and earth core of the wall) and its natural (nonintentional) destruction.

The relics of the fortifications of Vinoř were comparable in their characteristic construction (most recently, Boháčová & Dvořák, 2022) with the fortifications of nearly two dozen other sites in central Bohemia. Archeology associates them consistently (cf. Havrda & Podliska, 2022; Štefan & Boháčová, 2018; Varadzin, 2011) with the deep social transformation in central Bohemia that chronologically overlaps with the process of the

establishment of the central Bohemian realm of the oldest Czech dynasty, the Přemyslids (Kalhous, 2012).

5. Discussion

5.1. Fortification Characteristics Acquired from 2D ERT

2D profiling was able to identify all the major fortification features, as can be seen from Fig. 7, with ERT sections overlaid with sketches from the archeological excavations. Profiles with electrode spacings of 1 m delineated the ditch and rampart with visible internal structures and suggested the placement of the berm, as demonstrated in P2 acquired at T3 (Fig. 7A). More detailed 2D profiles (P20–P50) with electrode spacings of 0.5 m were more appropriate for the description of internal structures of the rampart due to higher resolution. The identification
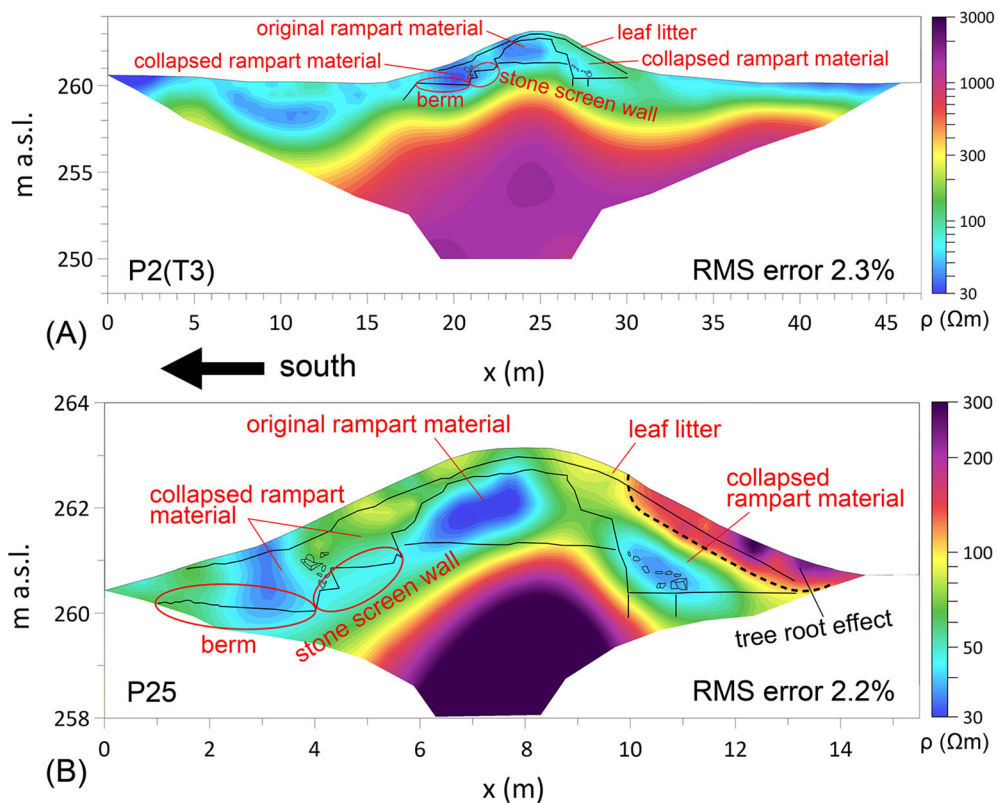
Figure 7
Comparison of archeological excavations with ERT sections. **A** P2 acquired at T3 with electrode spacing of 1 m. **B** P25 with detailed electrode spacing of 0.5 m. Both results captured all major fortification features. However, P2(T3) imaged the berm and sandstone basement better, while P25 showed in greater detail the inner structure of the rampart and identified more reliably the remains of the stone front wall

of a stone front wall was more reliable, remaining as a zone with higher resistivity within collapsed, low-resistivity material of the rampart (Fig. 7B), though the extent of the sandstone basement was affected by the small length of the profile and was better resolved in P1–P6.

5.2. Building Material Volume Estimation from 3D ERT

Estimation of the building material used for the fortification line was performed based on the approach proposed by Klanica et al. (2022a) from a 3D grid of P1–P6. Resistivity structures of the ditch and the rampart were separated from the final 3D resistivity model with the lowest RMS error of 2.77% based on particular resistivity thresholds, while volumes were calculated using ParaView software

(Fig. 4). The resistivity threshold for the ditch was chosen by inspecting the results from the time-lapse inversion and comparing the extent of the ditch anomaly on the 3D model with the time-lapse results. Since the berm was most likely covered by collapsed material of the rampart, it was included in the rampart's volume, and the ditch location was inferred to the x positions of 4–17.5 m. Finally, the value of 80 Ωm was selected (Fig. 4B), and the averaged calculated volume of the entire 5 m wide section for the 1 m wide strip of ditch filling was ca. 25.6 m^3.

The vertical and horizontal extents of the rampart's resistivity anomaly were almost constant through the time-lapse inversion results. The resistivity threshold value was selected in such a way that the structure included two low-resistivity anomalies separated by an area of higher resistivity, with the rear part of the rampart in the horizontal extent given

by the elevation profile of the rampart (x positions of 17.5–31 m). The value of 70 Ωm fit these criteria the best and was selected for the estimation of volume (Fig. 4C). The averaged calculated volume for a 1 m wide strip of rampart building material was ca. 19.6 m^3. It is supposed that inhabitants of the stronghold used excavated material from the ditch for the construction of the adjacent rampart, so both volumes should be roughly equal after the construction. However, the current volume of the rampart had to be smaller due to erosional and destruction processes.

Since the entire ditch was not excavated given its size, the calculated volume for the ditch could not be directly compared to the ground truth. The rampart volume inferred from the archeological section was ca. 18.9 m^3, which fit well with the volume of 19.6 m^3 obtained from the 3D ERT model. This averaged value was not exactly precise; however, it was close to the output of the archeological excavations, allowing us to infer the volume of the building material used in a nondestructive way. Considering the volume of building material derived from the 3D model and combining it with the length of the fortification (200 m), it was possible to estimate the total volume of dug-out material from the ditch as ca. 5120 m^3, while the rampart emerged from ca. 3920 m^3 of earth.

5.3. 4D ERT as a Key to Accurate Interpretation

The depth extent of the ditch remained almost constant through the time-lapse results (3.09–3.17 m, considering the 80 Ωm boundary) and made the interpretation more reliable. Major changes were observed in the case of the horizontal extent of the ditch, which was hardly recognizable after heavy rainfalls (Fig. 5 T2). In contrast, measurements performed under dry conditions clearly depicted the surrounding loess layer and rampart material and allowed us to delineate the horizontal extent of the ditch (Fig. 5 T1, T3, and T4). The constant appearance of a flat portion of bedrock between the ditch and rampart throughout the time-lapse results supported the presence of a berm. Two separate anomalies within the rampart were more visible after heavy rainfall (Fig. 5 T2) and made the presence of frontal screen wall stones clearer. Moreover, the

time-lapse survey confirmed the presence of a mid-resistivity anomaly at the x position of 30 m behind the rampart observed in P1-P3. It was present under all four moisture conditions and could be most likely attributed to a zone affected by the roots of trees growing near P1. Mature trees with extensive root systems are able to drain water from surrounding soil (Gea-Izquierdo et al., 2009; Metzger et al., 2018) and, correspondingly, raise soil resistivity. This idea was supported by the presence of three mature trees, which were growing only near the P1 position of x = 30 m, while rest of the rampart was covered by small bushes and trees not exceeding a height of 2 m.

Repeated measurements under different moisture conditions gave us the opportunity to evaluate changes in resistivity anomalies over time. Whereas static anomalies without resistivity changes support conclusions obtained from simple profiling, anomalies responding to moisture content offer deeper insight into examined features. Generally, 4D time-lapse measurements can significantly improve the understanding of the extent of individual resistivity anomalies in both vertical and horizontal directions and, consequently, develop interpretation. The presented results of the time-lapse inversions suggest that at least two surveys performed under different moisture conditions could offer a different perspective on the same profile. Time-lapse inversions considering time and space constraints also minimize the risk of inversion artifacts (Karaoulis et al., 2013), which can cause interpretations of nonexisting anomalies.

5.4. Quantitative Interpretation as a Substitute for Archaeological Excavations

The application of ERT within the interdisciplinary research of the outer fortification of the Vinoř stronghold was successful on two levels. Firstly, it was possible to select an optimal area for planned excavations based on the results of exploratory 2D profiles (P01–P03). The implementation of similar exploration fieldwork is not possible due to the costs, monument management, its size and ethics. Hence, exploratory profiling represents a crucial factor of subsequent archaeological research success. Secondly, the results of multidimensional ERT allowed

quantitative interpretation yielding a new quality of evidence for the internal structure of the fortification and its characteristics. For the last one hundred years, archaeology has been accustomed to working with clearly interpretable but difficult-to-obtain knowledge acquired exclusively by very expensive and nonrepeatable excavations. An affordable alternative in the form of complex ERT surveys significantly improve the amount of archaeological information gained by geophysics. ERT provided the noninvasive possibility of identifying structural characteristics of wood-and-earth wall with stone screening complemented by an outer ditch, which archaeology considers to be a basic formal manifestation of early medieval central locations in central Europe.

6. Conclusion

Complex ERT including 2D, 3D, and 4D (time-lapse) surveys were used for the characterization of a stronghold fortification with the intention of accessing quantitative interpretation. The results acquired from 2D profiles with 1 m electrode spacings were able to delineate a ditch and a rampart with a visible internal structure and suggested the placement of a berm. Better resolution and imaging of the stone front wall within the rampart was obtained from 2D profiles with 0.5 m electrode spacings. Understanding of the horizontal and vertical extents of the ditch, the berm, and the collapsed material of the rampart was significantly enhanced by a 4D time-lapse survey, which imaged the fortification line four times under different moisture conditions. Later, 3D modeling of the measured 2D profiles gave us access to the volume of building material used. The fortification line was subsequently excavated and analyzed by means of archaeology. Thus, the ERT results could be directly validated by the ground truth, and it was possible to establish better connections between resistivity images and individual construction components. A comparison of the joint ERT results with the excavations implied that a combination of different ERT survey types including the novel use of 4D time-lapse measurements in archaeology could significantly improve the amount of information gained. With this approach, both qualitative and quantitative interpretation is obtained and archaeological excavations can be replaced to a significant extent by geophysical methods so under certain circumstances cultural sites can be leaved intact for future generations.

Funding

Data Availability

All geophysical data presented here are available in standard industry formats from http://dx.doi.org/ https://doi.org/10.17632/45tw4fmkf6.1.

Declarations

Publisher's Note Springer Nature remains neutral with regard to jurisdictional claims in published maps and institutional affiliations.

REFERENCES

Abrams, M. E., & McCurdy, L. (2019). Massive assumptions and Moundbuilders - the history, method, and relevance of architectural energetics. In L. Mccurdy & M. E. Abrams (Eds.), *Architectural energetics in archaeology - analytical expansions and global explorations.* London and New York: Routledge.

AL-Hameedawi, M. M., Thabit, J. M., & AL-Menshed, F. H. (2022). Electrical resistivity tomography and ground-penetrating radar methods to detect archaeological walls of Babylonian houses near Ishtar temple, ancient Babylon city Iraq. *Geophysical Prospecting Early View.* https://doi.org/10.1111/1365-2478.13293

Al-Saadi, O.S., Schmidt, V., Becken, M., & Fritsch, T. (2018). Very-high-resolution electrical resistivity imaging of buried foundations of a Roman villa near Nonnweiler Germany. *Abstract Archaeological Prospection*, 25(3), 209–218. https://doi.org/10.1002/arp.1703

Ayachit, U. (2015). The paraview guide: A parallel visualization application, Kitware, ISBN 978-1930934306

Bernardini, F., Vinci, G., Forte, E., Mocnik, A., Višnjić, J., & Pipan, M. (2021). Integrating airborne laser scanning and 3D ground-penetrating radar for the investigation of protohistoric structures in Croatian Istria. *Applied Sciences, 11*, 8166. https://doi.org/10.3390/app11178166

Boháčová, I., & Dvořák, V. (2022). Hmotová rekonstrukce raně středověkého opevnění a jeho vývoje: proměny fortifikačních prvků z 9.-11. století ve výpovědi pramenů z někdejší Císařské konírny Pražského hradu a přilehlého dvora. *Archeologické Rozhledy, 74*(2), 241–274. https://doi.org/10.35686/AR.2022.10

Casas, A., Castanyer, P., Himi, M., Lovera, R., Rivero, L., Santos, M., Tremoleda, J., Sendrós, A., García-Artigas, R., & Urruela, A. (2021). Frequency Domain Electromagnetic mapping for delineating subsurface structures related to the historical port of Emporiae. *Archaeological Prospection, 29*, 33–43. https://doi.org/10.1002/arp.1834

Cau-Ontiveros, M. A., Mas-Florit, C., Chávez-Álvarez, E., Sala, R., Meyer, C., Ortiz-Quintana, H., & Rodríguez-Simón, P. (2023). Comprehensive geophysical prospection of the Roman and lateantique city of Pollentia (Alcúdia Mallorca Spain). *Archaeological Prospection.* https://doi.org/10.1002/arp.1900

Christensen, J. (2004). Warfare in the European neolithic. *Acta Archaeologica, 75*, 129–156. https://doi.org/10.1111/j.0065-001X.2004.00014.x

Corradini, E., Wilken, D., Zanon, M., Groß, D., Lübke, H., Panning, D., Dörfler, W., Rusch, K., Mecking, R., Erkul, E., Pickartz, N., Feeser, I., & Rabbel, W. (2020). Reconstructing the palaeoenvironment at the early mesolithic site of lake Duvensee: ground-penetrating radar and geoarchaeology for 3D facies mapping. *The Holocene.* https://doi.org/10.1177/0959683620902234

Cowan, E. A., Seramur, K. C., Costa, J. W., Bradley-Lewis, N., & Marshall, S. T. (2022). Integration of shallow geophysics, archaeology and archival photographs to reveal the past buried at Ingleside plantation, Piedmont North Carolina (USA). *Archaeological Prospection, 29*(4), 545–556. https://doi.org/10.1002/arp.1871

CUZK (State Administration of Land Surveying and Cadastre) (2017). Digital terrain model of the Czech Republic of the 5th generation (DMR 5G), https://ags.cuzk.cz/av/ (Accessed 5 October 2022)

De Smedt, P., Garwood, P., Chapman, H., Deforce, K., De Grave, J., Hanssens, D., & Vandenberghe, D. (2022). Novel insights into prehistoric land use at Stonehenge by combining electromagnetic and invasive methods with a semi-automated interpretation scheme. *Journal of Archaeological Science, 143*, 105557. https://doi.org/10.1016/j.jas.2022.105557

Desruelles, S., Chabrol, A., Hasenohr, C., Pavlopoulos, K., Apostolopoulos, G., Kapsimalis, V., Triantaphyllou, M., Koukousioura, O., Mathe, V., Chapoulie, R., & Fouache, E. (2023). Palaeogeographic reconstruction of the main harbour of the ancient city of Delos (Greece). *Journal of Archaeological Science, 160*, 105857. https://doi.org/10.1016/j.jas.2023.105857

Di Maio, R., La Manna, M., & Piegari, E. (2016). 3D Reconstruction of buried structures from magnetic, electromagnetic and ERT data: example from the archaeological site of Phaistos (Crete, Greece). *Archaeological Prospection, 23*, 3–13. https://doi.org/10.1002/arp.1516

Ellis, G. R., & Oldenburg, D. W. (1994). Applied geophysical inversion. *Geophysical Journal International, 116*, 5–11. https://doi.org/10.1111/j.1365-246X.1994.tb02122.x

Gea-Izquierdo, G., Montero, G., & Cañellas, I. (2009). Changes in limiting resources determine spatio-temporal variability in tree–grass interactions. *Agroforestry Systems, 76*, 375–387. https://doi.org/10.1007/s10457-009-9211-4

Grison, H., Klanica, R., Stejskalová, Š, & Šteffl, J. (2022). Geoelectric, magnetic susceptibility, and geochemical survey as a tool to clarify the origin of Bronze Age water reservoirs at the Štěpánov hillfort. *Czechia. Catena, 213*, 106192. https://doi.org/10.1016/j.catena.2022.106192

Günther, T., Rücker, C., & Spitzer, K. (2006). Three-dimensional modelling and inversion of dc resistivity data incorporating topography – II. Inversion. *Geophysical Journal International, 166*, 506–517. https://doi.org/10.1111/j.1365-246X.2006.03011.x

Havrda, J., & Podliska, J. (2022). Raně středověké opevnění Prahy: Archeologické nálezy z let 2002–2016 z Malé Strany. *Archeologie Ve Středních Čechách, 26*(2), 381–436.

Hegyi, A., Urdea, P., Floca, C., Ardelean, A., & Onaca, A. (2018). Mapping the subsurface structures of a lost medieval village in South-Western Romania by combining conventional geophysical methods. *Archaeological Prospection, 26*, 21–32. https://doi.org/10.1002/arp.1720

Holmes, J., Chambers, J., Meldrum, P., Wilkinson, P., Boyd, J., Williamson, P., Huntley, D., Sattler, K., Elwood, D., Sivakumar, V., Reeves, H., & Donohue, S. (2020). Four-dimensional electrical resistivity tomography for continuous, near-real-time monitoring of a landslide affecting transport infrastructure in British Columbia, Canada. *Near Surface Geophysics, 18*, 337–351. https://doi.org/10.1002/nsg.12102

Jeon, H. T., Hamm, S. Y., Lee, H. J., Park, S., & Kim, S. H. (2022). Delineating the Bonghwang earth castle and royal palace of Geumgwan Gaya kingdom using multiple geophysical techniques. *Archaeological Prospection, 29*(3), 465–478. https://doi.org/10.1002/arp.1867

Jo, Y. S., Lee, S. M., & Lee, Ch. H. (2018). Material characteristics and building technique for the rammed earth wall of the 13th Korean fortress in Ganghwa. *Environmental Earth Sciences, 77*, 617. https://doi.org/10.1007/s12665-018-7792-9

Kalhous, D. (2012). Anatomy of a duchy: the political and ecclesiastical structures of early Přemyslid Bohemia. Leiden: Brill, 2012. East Central and Eastern Europe in the Middle Ages, 450–1450. ISBN 978-90-04-22980-8.

Karaoulis, M., Tsourlos, P., Kim, J.-H., & Revil, A. (2013). 4D time-lapse ERT inversion: Introducing combined time and space constraints. Near Surface Geophysics, 12, 25–34. https://doi.org/10.3997/1873-0604.2013004

Kim, J. H., Yi, M. J., Park, S. G., & Kim, J. G. (2009). 4D inversion of DC resistivity monitoring data acquired over a dynamically changing earth model. Journal of Applied Geophysics, 68, 522–532. https://doi.org/10.1016/j.jappgeo.2009.03.002

Klanica, R., Grison, H., Šteffl, J., & Beránek, R. (2022a). Assessing volume of defensive structures for architectural energetics analysis using 3D electrical resistivity tomography. Remote Sensing, 14(11), 2652. https://doi.org/10.3390/rs14112652

Klanica, R., Křivánek, R., Grison, H., Tábořík, P., & Šteffl, J. (2022b). Capabilities and limitations of electrical resistivity tomography for mapping and surveying hillfort fortifications. Archaeological Prospection. https://doi.org/10.1002/arp.1857

Krivanek, R. (2021). The contribution of non-destructive geophysical surveys to archaeological research of early medieval hillforts in Bohemia: A case study of the Tismice hillfort area. Archaeological Prospection, 29(1), 87–101. https://doi.org/10.1002/arp.1839

Kuna, M., Krivanek, R., Chvojka, O., & Salkova, T. (2021). A quantitative approach to magnetometer survey data: The case of the late Bronze Age site of Breznice. Journal of Archaeological Science, 126, 105298. https://doi.org/10.1016/j.jas.2020.105298

Loke, M.H. (2020). Rapid 2-D Resistivity & IP inversion using the least-squares method. RES2DINV User's manual, Geotomo software. Accessed 2 September 2020 at www.geotomosoft.com

Loke, M. H., Acworth, I., & Dahlin, T. (2003). A comparison of smooth and blocky inversion methods in 2-D electrical imaging surveys. Exploration Geophysics, 34, 182–187. https://doi.org/10.1071/EG03182

Loke, M. H., & Barker, R. D. (1996). Rapid least-squares inversion of apparent resistivity pseudosections using a quasi-Newton method. Geophysical Prospecting, 44, 131–152. https://doi.org/10.1111/j.1365-2478.1996.tb00142.x

Loke, M. H., Dahlin, T., & Rucker, D. F. (2014). Smoothness-constrained time-lapse inversion of data from 3-D resistivity surveys. Near Surface Geophysics, 12, 5–24. https://doi.org/10.3997/1873-0604.2013025

McLachlan, P., Chambers, J., Uhlemann, S., Sorensen, J., & Binley, A. (2020). Electrical resistivity monitoring of river–groundwater interactions in a Chalk river and neighbouring riparian zone. Near Surface Geophysics, 18, 385–398. https://doi.org/10.1002/nsg.12114

Metzger, J.C., Kleemann, M., Weckmüller, J., Hildebrandt, A. (2018). Systematic patterns of forest soil water retention depending on the tree distance in a European mixed beech forest. 20th EGU general assembly, EGU2018, Vienna, proceedings from the conference p.9832.

Milo, P., Vágner, M., Tencer, T., & Murín, I. (2022). Application of geophysical methods in archaeological survey of early medieval fortifications. Remote Sensing, 14(10), 2471. https://doi.org/10.3390/rs14102471

Milo, P., Vavák, J., Vágner, M., Prišt'áková, M., Murín, I., & Tencer, T. (2020). Svätý Jur Neštich – new insights on the settlement and fortification of the early medieval hillfort. Študijné Zvesti Archeologického Ústavu Slovenskej Akadémie Vied, 67(1), 103–127. https://doi.org/10.31577/szausav.2020.67.5

Mozzi, P., Fontana, A., Ferrarese, A. N., Campana, S., & Francese, R. (2016). The Roman city of Altinum, Venice Lagoon, from remote sensing and geophysical prospection. Archaeological Prospection, 23, 27–44. https://doi.org/10.1002/arp.1520

Nowaczinski, E., Schukraft, G., Hecht, S., Rassmann, K., Bubenzer, O., & Eitel, B. (2012). A multimethodological approach for the investigation of archaeological ditches – exemplified by the early Bronze Age settlement of Fidvár Near Vráble (Slovakia). Archaeological Prospection, 19, 281–295. https://doi.org/10.1002/arp.1434

Nowaczinski, E., Schukraft, G., Rassmann, K., Hecht, S., Texier, F., Eitel, B., & Bubenzer, O. (2013). Geophysical-geochemical reconstruction of ancient population size – the early Bronze Age settlement of Fidvár (Slovakia). Archaeological Prospection, 20, 267–283. https://doi.org/10.1002/arp.1460

Nowaczinski, E., Schukraft, G., Rassmann, K., Reiter, S., Müller-Scheessel, N., Hecht, S., Eitel, B., Bubenzer, O., & Bátora, J. (2015). A multidimensional research strategy for the evaluation of settlement pits: 3D electrical resistivity tomography, magnetic prospection and soil chemistry. Archaeological Prospection, 22, 233–253. https://doi.org/10.1002/arp.1510

Oliva, M. (2004). Flint mining, rondels, hillforts. symbolic works or too much free time? Archeologické Rozhledy, 56, 499–531.

Parker, R. L. (1994). Geophysical inverse theory. Princeton University Press. ISBN 9780691036342.

Parkinson, W. A., & Duffy, P. R. (2007). Fortifications and enclosures in European prehistory: A cross-cultural perspective. Journal of Archaeological Research, 15, 97–141. https://doi.org/10.1007/s10814-007-9010-2

Pasteka, R., Panisova, J., Zahorec, P., Papco, J., Mrlina, J., Frastia, M., Vargemezis, G., Kusnirak, D., & Zvara, I. (2020). Microgravity method in archaeological prospection: Methodical comments on selected case studies from crypt and tomb detection. Archaeological Prospection, 27(4), 415–431. https://doi.org/10.1002/arp.1787

Pickett, J., Schreck, J. S., Holod, R., Rassamakin, Y., Halenko, O., & Woodfin, W. (2016). Architectural energetics for tumuli construction: The case of the medieval Chungul Kurgan on the Eurasian steppe. Journal of Archaeological Science, 75, 101–114. https://doi.org/10.1016/j.jas.2016.09.006

Ranieri, G., Sharpe, L., Trogu, A., & Piga, C. (2007). Time-lapse electrical resistivity tomography to delineate mud structures in archaeological prospections. Near Surface Geophysics, 5, 375–382. https://doi.org/10.3997/1873-0604.2007019

Rizzo, E., Dubbini, R., Clementi, J., Capozzoli, L., De Martino, G., Fornasari, G., Fiano, F. R., & Lombardi, M. (2023). Geomagnetic and FDEM Methods in the Roman. Heritage. https://doi.org/10.3390/heritage6020090

Rödder, T., & Kneisel, Ch. (2012). Permafrost mapping using quasi-3D resistivity imaging, Murtèl, swiss alps archaeological site of Bocca Delle Menate (Comacchio, Italy). Near Surface Geophysics, 10, 117–127. https://doi.org/10.3997/1873-0604.2011029

Rücker, C., Günther, T., & Spitzer, K. (2006). Three-dimensional modelling and inversion of dc resistivity data incorporating topography — I. Modelling. Geophysical Journal International, 166(2), 495–505. https://doi.org/10.1111/j.1365-246X.2006.03010.x

Salač, V., et al. (2019). Atlas pravěkých a raně středověkých hradišť' v Čechách. Archeologický ústav AV ČR Praha - ZBSA Schleswig.

Štefan, I., Boháčová, I. (2018). Early medieval fortified centres in Central Bohemia: key issues. In: Moravian and Silesian strongholds of the tenth and eleventh centuries in the context of Central Europe/Pavel Kouřil, Rudolf Procházka et al. Brno: The Czech academy of sciences, institute of archaeology, Brno s. 247–260. ISBN 978-80-7524-010-1.

Štefan, I., Hasil, J. (2023). Praha-Vinoř: proměny centrálního místa v zázemí středověké Prahy. (Průběžná zpráva). In: Krajina středověké Prahy, Jan Klápště, Tomáš Klír, Ivo Štefan (eds.). Praha, pp. 44–57.

Stele, A., Linck, R., Schikorra, M., & Fassbinder, J. W. E. (2022). UAV magnetometer survey in low-level flight for archaeology: Case study of a second world war airfield at Ganacker (lower Bavaria, Germany). *Archaeological Prospection, 29*(4), 645–650. https://doi.org/10.1002/arp.1877

Trebsche, P., Schlögel, I., & Flores-Orozco, A. (2022). Combining geophysical prospection and core drilling: reconstruction of a Late Bronze Age copper mine at Prigglitz- Gasteil in the Eastern Alps (Austria). *Archaeological Prospection.* https://doi.org/10.1002/arp.1872

Uhlemann, S., Dafflon, B., Peterson, J., Ulrich, C., Shirley, I., Michail, S., & Hubbard, S. S. (2021). Geophysical monitoring shows that spatialbheterogeneity in thermohydrological dynamics reshapes a transitional permafrost system. *Geophysical Research Letters, 48*, e2020GL091149. https://doi.org/10.1029/2020GL091149

Uhlemann, S., Ulrich, C., Newcomer, M., Fiske, P., Kim, J., & Pope, J. (2022). 3D hydrogeophysical characterization of managed aquifer recharge basins. *Frontier in Earth Science, 10*, 942737. https://doi.org/10.3389/feart.2022.942737

Varadzin, L. (2011). The development of Přemyslid domain strongholds in the heart of Bohemia: (a contribution to the discussion). In: Frühgeschichtliche Zentralorte in Mitteleuropa: internationale Konferenz und Kolleg der Alexander von Humboldt-Stiftung zum 50. Jahrestag des Beginns archäologischer Ausgrabungen in Pohansko bei Břeclav, 5.-9.10.2009, Břeclav, Tschechische Republik/hrsg. von Jiří Macháček, Šimon Ungerman. Bonn: Rudolf Habelt, 2011, s. 405–410.

Wallner, M., Doneus, M., Kowatschek, I., Hinterleitner, A., Kostelbauer, F., & Neubauer, W. (2022). Interdisciplinary investigations of the neolithic circular ditch enclosure of velm (lower Austria). *Remote Sensing, 14*(11), 2657. https://doi.org/10.3390/rs14112657

Zhang, Z., D-h, H., & Yao, Q. (2011). Quantitative interpretation for gas hydrate accumulation in the eastern Green Canyon Area, Gulf of Mexico using seismic inversion and rock physics transform. *Geophysics, 76*, B139–B150. https://doi.org/10.1190/1.3581358

Zhao, W., Tian, G., Lin, Q., Wang, X., Wang, Y., & Bie, K. (2019). Integrated characterization of ancient burial mounds using ERT and limited drillings at the Hepu Han Tombs in coastal area of Southern China. *Journal of Archaeological Science: Reports, 23*, 617–625. https://doi.org/10.1016/j.jasrep.2018.11.016

Zotti, G., Neubauer, W. (2011). Astronomical aspects of Kreisgrabenanlagen (Neolithic circular ditch systems) – an interdisciplinary approach. International symposium on archaeoastronomy proceedings IAU symposium 278